Strong and Ductile Colossal Carbon Tubes with Walls of Rectangular Macropores

Huisheng Peng,[1,2,*] Daoyong Chen,[3] Jian-Yu Huang,[4] S. B. Chikkannanavar,[2] J. Hänisch,[2] Menka Jain,[2] D. E. Peterson,[2] S. K Doorn,[2] Yunfeng Lu,[5,†] Y. T. Zhu,[6,‡] and Q. X. Jia[2,§]

[1]*The Institute for Advanced Materials & Nano Biomedicine, Tongji University, Shanghai 200092, China*
[2]*Los Alamos National Laboratory, Los Alamos, New Mexico 87545, USA*
[3]*Department of Macromolecular Science, Fudan University, Shanghai 200433, China*
[4]*Center for Integrated Nanotechnology, Sandia National Laboratories, Albuquerque, New Mexico 87185, USA*
[5]*Department of Chemical and Biomolecular Engineering, University of California as Los Angeles, California 90095, USA*
[6]*Department of Materials Science and Engineering, North Carolina State University, Raleigh, North Carolina 27695, USA*
(Received 21 February 2008; revised manuscript received 24 April 2008; published 3 October 2008)

We report a new type of carbon material—porous colossal carbon tubes. Compared with carbon nanotubes, colossal carbon tubes have a much bigger size, with a diameter of between 40 and 100 μm and a length in the range of centimeters. Significantly, the walls of the colossal tubes are composed of macroscopic rectangular columnar pores and exhibit an ultralow density comparable to that of carbon nanofoams. The porous walls of colossal tubes also show a highly ordered lamellar structure similar to that of graphite. Furthermore, colossal tubes possess excellent mechanical and electrical properties.

DOI: 10.1103/PhysRevLett.101.145501 PACS numbers: 61.46.−w, 62.25.−g, 81.07.De

The last 20 years in materials science have been marked by the revival of carbon-based materials [1]. Besides the conventional forms of carbon, graphite, and diamond, new forms of carbon have been discovered: fullerenes, carbon nanotubes, and carbon nanofoams [2–4]. Here we report a new type of carbon material we have recently discovered—porous colossal carbon tubes (CCTs). We have synthesized CCTs using a chemical vapor deposition (CVD) process. Briefly, a mixture of ethylene and paraffin oil (with kinematic viscosity of 33.5 centistokes or less at 40 °C) was used as the precursor. Ar with 6% H_2 was used to carry the precursor to a 1-inch quartz tube furnace where the growth took place in the temperature range of 750 and 850 °C. The CCT growth was carried out with 80 sccm ethylene and 120 sccm carrier gas in a typical synthesis. No catalyst was used. Figures 1(a) and 1(b) show typical scanning electron microscopy (SEM) images of the colossal tubes with diameters of ~50 μm. Energy-dispersive x-ray spectroscopy confirms that they are made of carbon. Note that some precipitates are shown on the outer surface of CCTs. These precipitates are made of amorphous carbon. Since their inner surface is always clean, we can conclude that these precipitates are produced after the formation of CCTs. In addition, the number of precipitates on the CCT increases with the increase of the growth time. For example, the outer surface of CCTs in Fig. 1(a) (grown for 30 min) has less precipitates and is much smoother than the one in Fig. 1(b) (grown for 3 h). The growth of amorphous carbon is similar to that in the synthesis of carbon nanotube arrays, in which a layer of amorphous carbon grows on the top of carbon nanotube arrays [5]. Figure 1(c) shows the Raman spectra of CCTs in Figs. 1(a) and 1(b). The strong D bands at ~1311 cm^{-1} correspond to the disordered features due to the finite particle size effect or lattice distortion of the graphite crystals, while the weak G bands at 1580 cm^{-1} of the tube in Fig. 1(a) and at 1590 cm^{-1} of the tube in Fig. 1(b) can be assigned to the E_{2g} first-order mode [6]. Note that the amorphous carbon on the outer surface of CCTs also contributes to the Raman spectra. The intensity ratio between the G band and the D band (I_g/I_d) decreases with the increase of the amorphous carbon. For example, the I_g/I_d decreases from 0.90 for the tube in Fig. 1(a) to 0.88 for that in Fig. 1(b). In addition, the G band shifts to a longer wavelength with the increase of the amorphous carbon since the G peak for the pure amorphous carbon appears at 1600 cm^{-1} [7].

The thickness of the tube wall is ~1.4 μm as shown in the cross-sectional image of SEM [Fig. 2(a)]. Interestingly, the wall is composed of rectangular columnar pores. The rectangular pores pass through the tube walls from one end to the other along the lengths of the tubes (i.e., along axial directions). While a pore height of ~1.2 μm is observed throughout the CCT, the width varies from 500 nm to 2 μm. This is confirmed by the side view of the wall by SEM [Fig. 2(b)]. A separation wall between neighboring column pores is also observed. The outer and inner shells of the CCT wall as well as the separation wall between the pores are ~100 nm in thickness. A high resolution transmission electron microscopy [TEM, Fig. 3(a)] further shows that the CCT wall has a layered graphite crystal structure, and the interlayer distance determined by an x-ray diffraction is 0.34 nm, which is the same as in the graphite [Fig. 3(b)].

It is well known that the porous structure (with a density of 2–10 mg/cm^3) in carbon nanofoams makes them extremely light [8]. Similar to carbon nanofoams, the macroporous CCTs are ultralight as well: CCTs with a pore size of 950 nm × 1200 nm and an outer diameter of 54.5 μm are calculated from the SEM image to have a density of 11 mg/cm^3, which is almost comparable to the density of

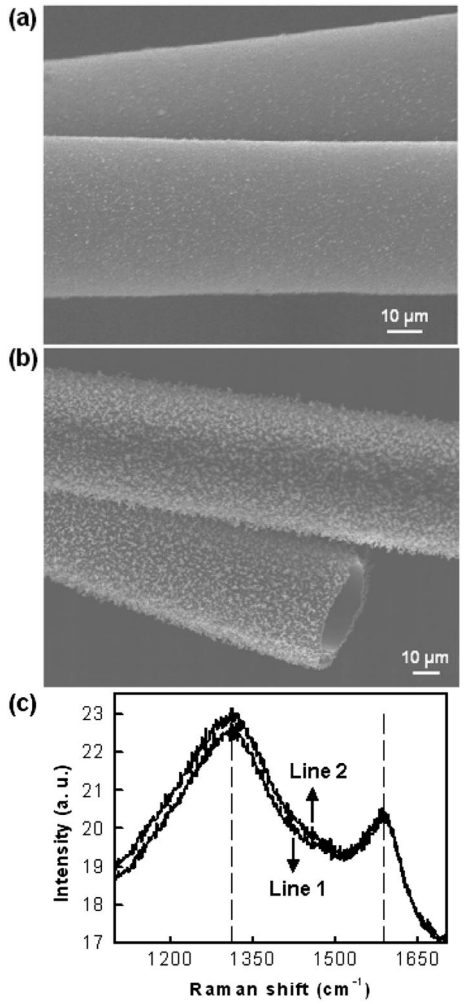

FIG. 1. (a) Scanning electron microscopy (SEM) image of colossal carbon tubes (CCTs) grown for 30 min. (b) SEM image of CCTs grown for 3 h. (c) Raman spectra of CCTs. Lines 1 and 2 correspond to the tubes in (a) and (b), respectively.

carbon nanofoams. The density of the CCT wall is calculated to be 116 mg/cm^3. It is very difficult to directly measure the weight of individual CCTs with appropriate accuracy due to their ultralight weights. These unique properties of CCTs offer many potential applications such as in electrochemical devices [9].

Carbon nanotubes, with a tensile strength of up to 100 GPa, are the strongest material ever discovered [10]. To exploit this superior property for practical applications, individual carbon nanotubes have been assembled into macroscopic fibers [11,12]. However, these macrofibers show a very low tensile strength of less than 3.3 GPa [12–15]. This is mainly due to the clustering of nanotube ends, internanotube slippage and intrananotube defects. In contrast, the CCTs have demonstrated much improved mechanical properties compared to carbon nanotube fibers of similar sizes. Figure 4(a) shows the maximum tensile strength of ~6.9 GPa of a CCT. The cross-sectional areas

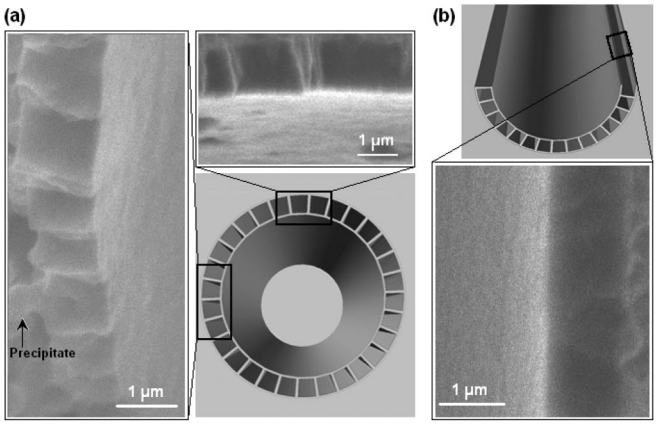

FIG. 2. (a) Schematic illustration and SEM images corresponding to the specific positions in the scheme by the top view of a tube. Precipitates are observed on the outer surface of the tube wall, shown by the arrow. (b) Schematic illustration and a corresponding SEM image by the side view of the tube wall. Schemes in (a) and (b) are drawn by the AUTOCAD Software based on experimental results.

of the CCT used to calculate the tensile strengths are determined by SEM and calculated as the area between the inner and the outer shells of the CCT wall. The mechanical properties of CCTs were characterized using a Shimadzu Universal Testing Instrument with a 5 N load cell. The test process is similar to carbon nanotube fibers [16]. Briefly, for each measurement an individual CCT with gauge length of 5 mm was first mounted on a paper tab and tested under tension at a displacement speed of 0.05 mm/s.

The specific strength and tenacity are important mechanical properties of materials. Both of them represent the ratio of strength over density and can be converted into each other. In our case, the combination of high strength and low density renders the CCT a high specific strength and tenacity. The specific strength usually has a unit of cm. For example, the CCT in Fig. 4 has a strength of 6.9 GPa and a density of 0.116 g/cm^3,the specific strength is then calculated as (6.9 GPa)/(0.116 g/cm^3) $= 6.07 \times 10^8$ cm. This is about 15 times that of the strongest carbon fiber (T1000). The unit of tenacity is g/tex, in which tex is defined as the weight in grams per 1000 m length, so 1 g/tex $= 10^5$ cm. Therefore, the tenacity of the CCT in Fig. 4 is 6.07×10^3 g/tex, which is about 30 times that of Kevlar [17] and 224 times that of individual cotton fibers [18].

Interestingly, Fig. 4(a) also shows that the CCT deforms under the tensile force in a ductile manner and the diameter undergoes a continuous local shrinkage before breaking, much like the deformation of a ductile metal wire. This is in sharp contrast to the typical brittle fracture of advanced fibers. This ductile behavior is attractive to many applications where high toughness is desired. Figure 4(b) further shows the diameter decrease of a CCT from 83 to 63 μm

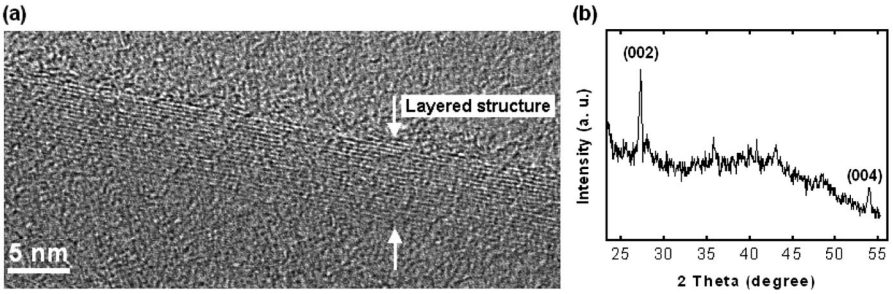

FIG. 3. (a) Layered structure of the tube wall, observed by a high resolution transmission electron microscopy. (b) A typical x-ray diffraction pattern.

during the deformation. The CCT maintains its round shape during this deformation process. In addition, Fig. 4(a) shows that the CCT sustained about 3% strain before fracture. This deformation behavior might have resulted from CCT's unique porous architecture and the lamellar structure in the solid part of the wall.

The electrical conductivity of individual CCTs is $\sim 10^3$ S/cm at room temperature compared with $\sim 10^2$ S/cm for multiwalled carbon nanotube fibers [19,20]. The conductivities of individual CCTs along axial directions with temperature have also been measured, and the experimental details on the preparations of samples have been reported before [19]. Figure 5 shows the temperature dependence of the conductivity of a CCT. Obviously, the conductivity increases with the temperature, suggesting a semiconducting behavior [21].

Deriving a clear mechanism for the formation of such CCTs is still a challenge. SEM characterizations (images not shown here) show that some graphite sheets curve up but do not form complete tubes, indicating that these CCTs are formed by the scroll of graphite sheets during the CVD growth process. Based on these observations, we hypothesize the following process for the formation of CCTs (see Fig. 6). First, large graphite sheets with rectangular macropores in the wall are nucleated. The two surface walls of the sheet grow at different rates, forcing the graphite sheets to curl up. When the two edges of a sheet meet and join together, a tubular morphology forms (see Fig. 1). However, if the two edges do not meet, a scrolled structure or an incomplete tube may be formed. If the two surface walls grow at the same rate, a flat graphite sheet will be produced. Both scrolled and flat sheets have been confirmed by SEM. It is not clear why the two wall surfaces grow at different rates. One possibility is that there is a gradient in the concentration of the carbon source above the quartz substrate on which the CCTs are synthesized. This gradient may have been caused by the laminar flow of carbon source gases whose flow rate becomes lower near the stationary substrate surface. It should be noted that the high resolution TEM in Fig. 3(a) is observed from a cross-sectional view, which shows that the graphitic layered structures are oriented along the circumferential direction. Similar assembly behaviors have been reported in some other carbon and organic systems [22–25]. More effort is under way to further investigate these issues and the formation of the rectangular macropores.

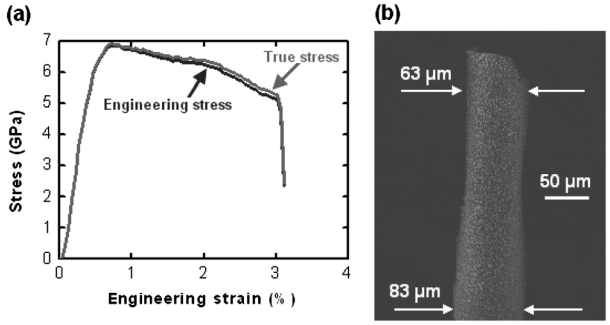

FIG. 4. Mechanical properties of the CCT. (a) Curves of engineering and true stresses vs engineering strain, showing a high tensile strength of 6.9 GPa. The engineering stress and strain are defined as the load divided by the original cross-sectional area and the elongation divided by the original length of the sample, respectively [26]. The true stress is defined as the load divided by the *in situ* cross-sectional area. The cross-sectional area of the CCT was calculated as the area between the inner and outer walls. (b) SEM image of the breaking part under tensile stress.

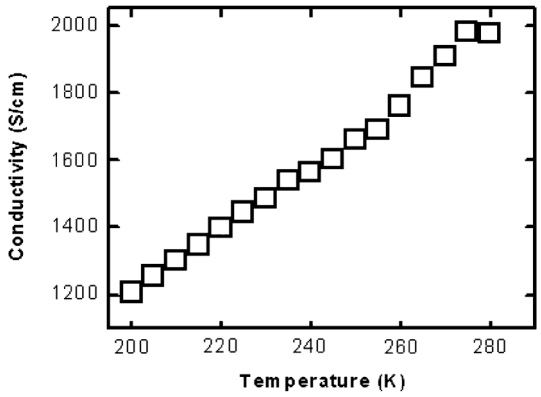

FIG. 5. Temperature dependence of the electrical conductivity in a CCT.

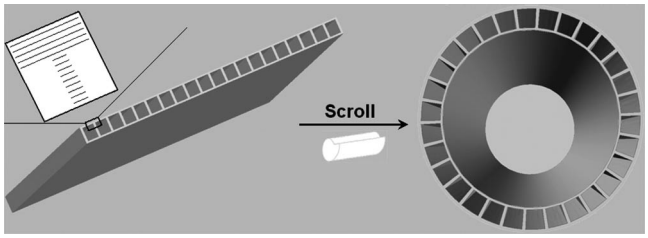

FIG. 6. Schematic illustration of the formation of a CCT scrolled from a macroporous graphite sheet.

The CCTs synthesized here have a unique architecture with rectangular macropores across the tube walls and layered crystal structures in the solid walls. This unique architecture renders them a combination of superior properties, including ultralight weight, extremely high strength, excellent ductility, and high conductivity. These unique architectural and physical properties give them great potentials for a variety of advanced applications. For example, the diameter and the length of CCTs are comparable to those cotton fibers and the tenacity of the CCTs is 224 times that of cotton fibers. This suggests that conventional textile technologies can be used to make CCT fabrics that are much stronger than any current fabrics for applications such as body armors and lightweight, high strength composite structures. Other potential applications include making *in situ* self-healing composite structures, medical devices to deliver/release multiple drugs simultaneously, and microelectromechanical systems, to name only a few.

This work was partially supported as a Los Alamos National Laboratory Directed Research and Development Project under the United States Department of Energy. This work was performed, in part, at the Center for Integrated Nanotechnologies, a U.S. Department of Energy, Office of Basic Energy Sciences user facility. Sandia National Laboratories is a multiprogram laboratory operated by Sandia Corporation, a Lockheed-Martin Company, for the U.S. Department of Energy under Contract No. DE-AC04-94AL85000.

*Corresponding author.
penghs2004@yahoo.com

†Corresponding author.
luucla@ucla.edu

‡Corresponding author.
ytzhu@ncsu.edu

§Corresponding author.
qxjia@lanl.gov

[1] T. D. Burchell, *Carbon Materials for Advanced Technologies* (Pergamon, Oxford, U.K., 1999).
[2] H. W. Kroto, J. R. Heath, S. C. O'Brien, R. F. Curl, and R. E. Smalley, Nature (London) **318**, 162 (1985).
[3] S. Iijima, Nature (London) **354**, 56 (1991).
[4] A. V. Rode, E. G. Gamaly, and B. Luther-Davies, International Patent Application No. PCT/AU98/00739, priority date 11 September, 1997.
[5] H. Peng *et al.* (unpublished).
[6] T. Luo, J. Liu, L. Chen, S. Zeng, and Y. Qian, Carbon **43**, 755 (2005).
[7] S. V. Subramanyam, A. Sayeed, V. Meenakshi, S. Bhattacharya, A. Cholli, and S. J. Tripathi, Appl. Phys. **81**, 2907 (1997).
[8] A. V. Rode *et al.*, Phys. Rev. B **70**, 054407 (2004).
[9] A. E. Fischer, K. A. Pettigrew, D. R. Rolison, R. M. Stroud and J. W. Long, Nano Lett. **7**, 281 (2007).
[10] Q. Li *et al.*, Adv. Mater. **18**, 3160 (2006).
[11] M. Zhang *et al.*, Science **309**, 1215 (2005).
[12] A. B. Dalton *et al.*, Nature (London) **423**, 703 (2003).
[13] X. Zhang *et al.*, Adv. Mater. **19**, 4198 (2007).
[14] P. Miaudet *et al.*, Nano Lett. **5**, 2212 (2005).
[15] H. Peng, M. Jain, Q. Li, D. E. Peterson, Y. T. Zhu, and Q. X. Jia, J. Am. Chem. Soc. **130**, 1130 (2008).
[16] X. Zhang, Small **3**, 244 (2007).
[17] A. Kelly, *Concise Encyclopedia of Composite Materials* (Pergamon, Oxford, U.K., 1995).
[18] C. A. Lawrence, *Fundamentals of Spun Yarn Technology* (CRC Press, New York, 2003).
[19] Q. Li *et al.*, Adv. Mater. **19**, 3358 (2007).
[20] L. B. Zhu *et al.*, Carbon **44**, 253 (2006).
[21] H. Peng, J. Am. Chem. Soc. **130**, 42 (2008).
[22] Y. Luo, J. Lin, H. Duan, J. Zhang, and C. Lin, Chem. Mater. **17**, 2234 (2005).
[23] H. Peng, Y. Zhu, D. E. Peterson, and Y. Lu, Adv. Mater. **20**, 1199 (2008).
[24] J. P. Hill *et al.*, Science **304**, 1481 (2004).
[25] T. Yamamoto *et al.*, J. Am. Chem. Soc. **128**, 14337 (2006).
[26] W. F. Smith and J. Hashemi, *Foundations of Materials Science and Engineering* (McGraw-Hill Higher Education, Boston, 2006), 4th ed.